Study on the characteristics and properties of composites based on PLA/TiO$_2$ and thermoplastic starch

Tran Thi Mai[*], Nguyen Thi Thu Trang, Nguyen Thuy Chinh, Do Quang Tham, Tran Huu Trung, Thai Hoang

*Institute for Tropical Technology, Vietnam Academy of Science and Technology,
18 Hoang Quoc Viet, Cau Giay, Ha Noi, Viet Nam*

[*]Email: *tranmai.k55@gmail.com*

Abstract. The purpose of this study is to fabricate composites based on poly(lactic acid) (PLA), thermoplastic starch (TPS) and TiO$_2$ nanoparticles (n-TiO$_2$), and to investigate the effects of TiO$_2$ on the interface compatibility of TPS and PLA. The FTIR spectra confirmed that the interfacial interaction between the components is the formation of hydrogen bonding between TiO2 and PLA/TPS matrix (Ti-O-C bond). The results indicated that the tensile properties of PLA/TPS blends were strongly influenced by the PLA/TPS ratio which decreased with increasing TPS content. Besides, the tensile strength of the composites was improved in the presence of n-TiO$_2$ particles due to the high crystallinity of the PLA/TPS/n-TiO$_2$ composites (with an n-TiO$_2$ content of 1 wt.%) in comparison with the PLA/TPS blends as shown in DSC and XRD analysis. The TGA results also indicated that the thermal stability of the PLA/TPS/n-TiO$_2$ composites was improved with the addition of TiO$_2$ nanoparticles. Finally, SEM images indicated that TiO$_2$ nanoparticles were well dispersed in the PLA/TPS matrix at low TiO$_2$ content. At high TiO$_2$ content (2 wt.%) it caused agglomeration into clusters which reduced the properties of the composites.

Keywords: Poly(lactic acid), thermoplastic starch, titanium dioxide.

Classification numbers: 2.4.2, 2.9.3, 2.9.4

1. INTRODUCTION

Recently, the impact of plastic waste is a concern worldwide. Therefore, research on biodegradable materials is receiving increasing attention. Biodegradable and renewable polymers have attracted strong attention due to their effects on reducing environmental pollution. Poly(lactic acid) (PLA) belongs to the aliphatic polyester family and is one of the eco-friendly polymers that has been widely used for the production of biodegradable, biocompatible, nontoxic materials [1 - 4]. The PLA is derived from renewable biomass products and wastes such as corn, starch, sugar, etc. [5 - 7]. It is a thermoplastic polyester and one of the most popular biodegradable polymers with stiffness, strength and gas permeability comparable to those of synthetic polymers (petroleum based plastics) such as polypropylene (PP), poly(ethylene terephthalate) (PET) and polystyrene (PS). Because of its biodegradability, it is an

alternative to other non-biodegradable polymers in some applications by improving the negative environmental effects of non-biodegradable polymers. In a humid environment, especially in the presence of acids and bases, the PLA is easily hydrolyzed. However, its application is also limited by its low degradation rate (compared to other natural polymers), relatively high cost and brittleness [8]. Therefore, it is proposed to overcome the low degradation rate of PLA by blending with other natural polymers with high degradation rates including polysaccharides, such as cellulose, chitin, glycogen and starch. Among these materials, starch is considered one of the most promising candidates to improve the biodegradability of PLA, due to its low cost, abundance and availability from various plant sources. However, starch has a limitation that is its poor processability due to its melting point being higher than its decomposition temperature. To enhance its handling, starch is often gelatinized with plasticizers like glycerol, water, urea, citric acid, sorbitol and sugars, etc. [9 - 12], and the obtained compound is called thermoplastic starch (TPS).

Titanium dioxide (TiO_2) has been attracting interest in various fields due to its photocatalytic and antibacterial activity [13]. Apart from the antibactericidal properties of TiO_2, its biocompatibility and small size when used in nanocomposite form help improve the catalytic effect of this material. Therefore, the decomposition ability of nanocomposites containing TiO_2 under solar radiation or UV light can be significantly increased. The irradiation of TiO_2 by light with energy greater than the band gap of TiO_2 will lead to the formation of electron-hole pairs, causing a redox reaction on the TiO_2 surface. This transition favors the oxidative capacity of other species by generating active agents like radicals. There have been many studies on PLA/TiO_2 nanocomposites. They have good mechanical, thermal and photocatalytic properties, and have many potential applications in fields such as adsorption and photocatalysis for the removal of environmental pollutants, coatings, biosensors, etc. Toniatto *et al.* studied the development of PLA/TiO_2 nanocomposites with high anti-bacterial properties by electrospinning method [14]. Pattarnaphong Chanklom *et al.* investigated the application of anatase formed TiO_2 as a photocatalyst for PLA matrix by solution casting method [15]. Yanbing Luo *et al.* studied on the preparation of PLA/TiO_2 photodegradable materials that can be used as environmentally friendly materials [16].

The inclusion of photodegradable substances such as TiO_2 and fast biodegradable substances such as starch/thermoplastic starch promotes the decomposition process under all conditions and speeds up the rate of biodegradation. Besides, some properties and characteristics of PLA will be changed. The purpose of this research is to prepare biodegradable composites based on PLA, TPS and TiO_2 nanoparticles by melt-blending method. The effects of TiO_2 on the decomposition as well as the characteristics, properties, and morphology of the composites were investigated by a combination of Fourier transform infrared (FTIR) spectrophotometry, X-ray diffractometry (XRD), differential scanning calorimetry (DSC), thermogravimetric analysis (TGA) and tensile tester.

2. EXPERIMENTAL

2.1. Materials

Polylactic acid - PLA (2002D grade) with a density of 1.24, M_n of 110 KDa, a melt flow index (MFI) of 5 - 7 g/10 min at 210 °C and a load of 2.16 kg was purchased from Nature Works (USA). Thermoplastic starch (TPS) was a commercial product of China. Titanium dioxide (TiO_2) powder with a particle size of about 12 nm was supplied by Sigma-Aldrich Co. (USA).

2.2. Preparation of PLA/TPS/TiO$_2$ nanocomposites

The formulation of PLA/TPS/nano TiO$_2$ (n-TiO$_2$) composites and their abbreviations are presented in Table 1. Materials such as PLA and TPS were pre-treated by drying at 40 °C for 24 hours to eliminate water possibly absorbed on the surface of the particles before being used. The composites of PLA/TPS/n-TiO$_2$ were melt mixed at 175 °C for 5 minutes under a screw speed of 50 rpm using a Haake Rheomix 610 machine (Germany). After melt mixing, the blends were molded into bar shapes by a Haake Minijet Pro machine (Germany) at 175 °C, a pressing pressure of 400 bar for 10 seconds. The sample of bar shapes was allowed to cool and stored at room temperature for at least 24 hours before determining its physicochemical properties.

Table 1. Formulation of PLA/TPS/n-TiO$_2$ composites.

Sample	PLA (g)	TPS (g)	TiO$_2$ (g)
PT 91	65.39	7.27	-
PT 82	59.46	14.87	-
PT 73	53.39	22.88	-
PT 64	46.75	31.17	-
PTT 911	65.05	7.22	0.73
PTT 912	64.40	7.26	1.45
PTT 821	59.09	14.50	0.74
PTT 822	58.72	14.13	1.48

2.3. Characterization and methods

2.3.1. FTIR spectra

FTIR spectra of the samples were recorded using reflectometry mode on an infrared spectrometer - Nicolat iS10 (USA) with the following measuring conditions: resolution 16 cm^{-1}, number of scans 32, wavelengths from 4000 cm^{-1} to 400 cm^{-1} at room temperature.

2.3.2. Tensile properties

The tensile strength and elongation at break of the PLA/TPS/n-TiO$_2$ composites were determined at a speed of 50 mm/min according to ASTM D638 using a Zwick Tensile 2.5 machine (Germany) under ambient conditions. The specimens had a bar shape with a length of 60 mm, a width of 12.7 mm and a thickness of 1 mm. The results reported were the average value of 5 measurements.

2.3.3. Thermal properties

Thermogravimetric analysis (TGA) of the PLA/TPS/n-TiO$_2$ composites was investigated on the TGA209F1 instruments of NETZSCH (Germany). Analyses were performed under nitrogen atmosphere and heated from room temperature to 600 °C at a heating rate of 10 °C/min.

Differential scanning calorimetry (DSC) of the PLA/TPS/n-TiO$_2$ composites was performed in the DSC204F1 instruments of NETZSCH (Germany). The mass of the sample was weighed to be 7-10 g and heated from room temperature to 300 ^{o}C. The degree of crystallinity (χ_c) was calculated from the DSC curves as follows:

$$\chi_c = \frac{\Delta H_m - \Delta H_c}{\Delta H_f \; x \; (1 - \alpha)} \times 100\%$$

where, ΔH_m and ΔH_c are the enthalpy of melting and crystallization (J/g) that was calculated from the DSC curves. ΔH_f is the heat of fusion for the completely crystallized PLA (93.1 J/g), and α is the weight fraction of TPS and TiO$_2$ in the blends [17].

2.3.4. X-ray diffraction

The crystal structure of the PLA/TPS/n-TiO$_2$ composite film was determined by X-ray diffraction technique. It was performed with Cu - Kα1 radiation (λ = 1.54060 Å) on a Bruker - AXS D5005 equipment. The XRD patterns were recorded in the range of 2θ from 10 to 70° at ambient temperature.

2.3.5. Morphology

The morphology of the sample surfaces was evaluated by scanning electron microscopy (SEM) images recorded with a JEOL SM-6510 scanning electron microscope (Japan) at room temperature. All specimens were coated with a thin layer of platinum to increase conductivity.

3. RESULTS AND DISCUSSION

3.1. FTIR spectra

Figure 1 illustrates the FTIR spectra of PLA/TPS and PLA/TPS/n-TiO$_2$ composites, respectively. In the spectra of the PLA/TPS blends, there are peaks at wavenumbers of 3400 - 3500 cm^{-1}, corresponding to the stretching vibration of the O-H moiety in the carboxyl groups. The peaks corresponding to the stretching vibration of C-H and C=O groups are observed in the bands from 2770 to 3000 cm^{-1} (2944 cm^{-1}) and the band at 1750 cm^{-1}, respectively. The peaks at 950 and 1460 cm^{-1} are attributed to the stretching vibrations of the CH$_3$ and C-CH$_3$ groups (with antisymmetry at 1455 cm^{-1} and symmetry at 1370 cm^{-1}) [18]. Compared with neat PLA, the absorption peaks at 2927 cm^{-1} and 1743 cm^{-1} shift toward a higher wavenumber, confirming the interfacial interaction (the formation of hydrogen-bonding) between PLA and TPS. The other samples with different PLA:TPS ratios have similar FTIR spectra of the PLA/TPS/n-TiO$_2$ composites.

In the spectra of the PLA/TPS/n-TiO$_2$ composites, the characteristic peaks for the stretching vibrations of the Ti-O and Ti-O-Ti groups can be observed in the region between 1383 and 1650 cm^{-1} [19-20]. There are some differences observed in the spectra of the PTT samples because the peaks of hydroxyl group and -CH$_3$ group shift towards higher wavenumbers. This indicates the interfacial interaction between the components as the formation of hydrogen bonding between the nanoparticles and the PLA/TPS matrix. Overall, in the FTIR spectrum of PTT composites, new bands appear due to the presence of TiO$_2$ (such as the bands at about 1383 and 1650 cm^{-1}). All these bands are shifted from their original position in PLA. This indicates the interaction of PLA with the surface of n-TiO$_2$ through hydrogen-bonding**.**
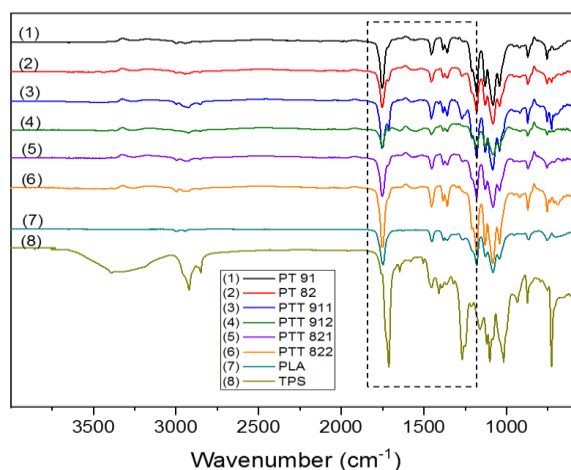
Figure 1. FTIR spectra of PLA, TPS, PLA/TPS and PLA/TPS/n-TiO$_2$ composites.

3.2. Tensile properties

Table 2. Tensile properties of PLA/TPS/n-TiO$_2$ composites.

Sample	Tensile strength (MPa)	Elongation at break (%)
PLA	42.62 ± 3.55	3.89 ± 0.42
PT 91	27.66 ± 2.33	4.36 ± 0.59
PT 82	26.06 ± 3.31	2.27 ± 0.21
PT 73	20.47 ± 1.33	1.32 ± 0.16
PT 64	19.96 ± 3.34	1.59 ± 0.24
PTT 911	29.86 ± 1.82	2.22 ± 0.45
PTT 912	28.28 ± 1.94	1.94 ± 0.32
PTT 821	26.68 ± 2.21	1.20 ± 0.09
PTT 822	22.07 ± 1.62	2.20 ± 0.17

Table 2 shows the tensile strength and elongation at break of the PLA/TPS/n-TiO$_2$ composites. It can be seen that the tensile strength of the PLA/TPS blends (PT samples) tends to decrease with increasing the weight fraction of TPS up to 40 wt.%, such as decreasing from 27.66 MPa to 19.96 MPa corresponding to increasing the TPS content from 10 to 40 wt.%. The decrease in tensile properties of the PLA/TPS blends is due to the fact that TPS has a much lower tensile strength than the neat PLA. Table 2 also shows that the tensile strength is improved in the presence of TiO$_2$ nanoparticles, for example the tensile strength is increased from 27.66 to 29.86 MPa (PTT 911). This proves that the components interact well, and the adhesion between the surfaces of n-TiO$_2$ particles is improved. However, the tensile strength of the composites slightly is decreased with increasing TiO$_2$ content up to 2 wt.% due to phase separation.

Similarly, the elongation at break of the PT samples gradually is decreased from 4.36 to 1.59 % when TPS content is increased from 10 to 40 wt.%. In particular, the PT 73 sample (with

a TPS content of 30 wt.%) reaches the lowest point of 1.32 %. From Table 2, it is clearly seen that the elongation at break of all samples are low, and reaches the maximum value of 4.36 % for the sample PT 91. This is because both PLA and TPS are brittle in nature. In addition, the elongation at break of PLA/TPS/n-TiO$_2$ composites tends to decrease upon the addition of n-TiO$_2$. For example, it is reduced from 4.36 to 2.22 % (PTT 911) and from 2.27 to 1.20 % (PTT 821). This can be explained by the fact that n-TiO$_2$ particles are phase separated and agglomerate to form defects in composite leading to a reduction in the tensile properties of the PLA/TPS/n-TiO$_2$ composites.
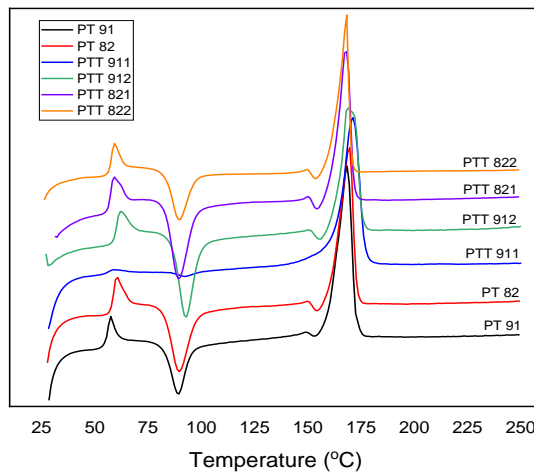
3.3. DSC analysis and crystallization behavior

Figure 2. DSC curves of PLA/TPS and PLA/TPS/n-TiO$_2$ composites.

Figure 2 shows the DSC curves of PLA/TP/n-TiO$_2$ composites (PT 91, PT 82, PTT 911, PTT 912, PTT 821 and PTT 822), observing a dependence of the glass transition temperature (T$_g$) of PLA on the composition of the blends. The T$_g$ increases slightly from 57.5 to 60.3 $^{\circ}$C when TPS content increases from 10 to 20 wt.%. Similarly, the T$_g$ also is increased slightly with increasing n-TiO$_2$ content, which indicates an extended compatibility between the components of the composites. Table 3 presents all the DSC data and the degree of crystallinity (χ_c) of the PLA-based composites. It can be seen that by adding n-TiO$_2$ to the PLA/TPS blends, the crystallization temperature (T$_c$) of the blends is changed. The peak temperature T$_c$ of the PT blend is 89.2 $^{\circ}$C, while that of the PTT 911 composite is 92 $^{\circ}$C. Besides, the melting temperature (T$_m$) of the PLA/TPS/n-TiO$_2$ composite also shifts to a high temperature due to the addition of n-TiO$_2$ particles to the PLA/TPS blend. The peak temperature T$_m$ of the PLA/TPS blends is about 168 $^{\circ}$C, while that of the PTT composite is 171 $^{\circ}$C. Table 3 also indicates that the degree of crystallinity (χ_c) of the PLA/TPS blends tends to decrease as the TPS content increases. For examples, the χ_c of the PLA/TPS blends decreases from 40.11 % (PT 91) to 35.48 % (PT 82). On the other hand, the χ_c of the PLA/TPS/n-TiO$_2$ composites is increased when adding n-TiO$_2$ particles to the PLA/TPS matrix. This may be attributed to the better dispersion and interfacial effect of n-TiO$_2$ particles with the PLA/TPS matrix, which improves the χ_c of the composite. However, when the content of n-TiO$_2$ particles increases from 1 wt.% to 2 wt.%, the χ_c of the PLA/TPS/n-TiO$_2$ composites is decreased, for example, the χ_c decreases from 59.67 % (PTT 911) to 51.63 % (PTT 912) and from 35.76 % (PTT 821) to 32.59 % (PTT 822). This is due to

the fact that the n-TiO$_2$ particles are disrupted regularly in the structure of the PLA chains, increasing the spacing between the chains.

Table 3. DSC data of PLA/TPS and PLA/TPS/n-TiO$_2$ composites.

Sample	Glass transition temperature T$_g$ (^{o}C)	Crystallization temperature T$_c$ (^{o}C)	Melting temperature T$_m$ (^{o}C)	Melting enthalpy ΔH$_m$ (J/g)	Crystallization enthalpy ΔH$_c$ (J/g)	Degree of crystallinity χ$_c$ (%)
PLA	58	-	153	29.4	4.98	26.22
TPS	68.2	-	132.3	42.14	-	28.90*
PT 91	57.5	89.2	168.3	36.39	6.514	40.11
PT 82	60.3	89.6	169.4	27.95	2.185	35.48
PTT 911	58.8	92.2	171.0	51.16	1.715	59.67
PTT 912	62.2	92.6	168.6	43.26	2.349	51.63
PTT 821	58.9	89.3	167.7	35.21	5.913	35.76
PTT 822	59.2	89.6	168.1	31.04	7.071	32.59

* Degree of crystallinity of TPS was determined using XRD diffraction [21, 22].
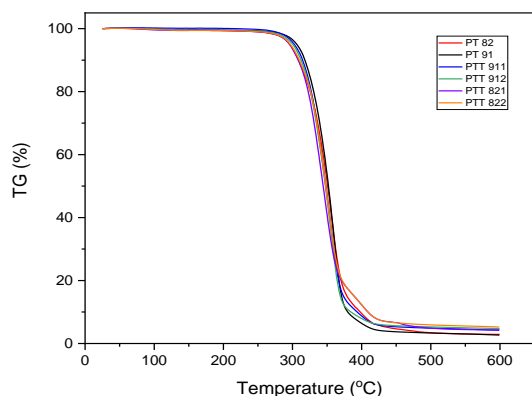
3.4. Thermal gravity analysis (TGA)

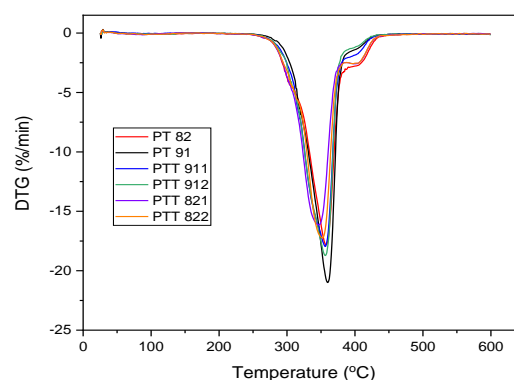*Figure 3.* TGA curves of PLA/TPS and PLA/TPS/n-TiO$_2$ composites.

Figure 4. Differential thermogravimetric (DTG) curves of PLA/TPS/n-TiO$_2$ composites.

Figure 3 presents the TGA curves of PLA/TPS (PT 91 and PT 82) and PLA/TPS/n-TiO$_2$ (PTT 911, PTT 912, PTT 821 and PTT 822) composites. All samples show negligible weight loss in the temperature range from ambient temperature to 300 ^{o}C, they are then continuously decomposed at higher temperatures and completely decomposed at about 500 ^{o}C. The onset decomposition temperature (T$_{on}$) of PLA composites is about 177 ^{o}C. The TG data and the weight percentage of the residue at different temperatures are reported for all samples in Table 4. The highest decomposition temperature (T$_{max}$) of the PLA/TPS/n-TiO$_2$ composites is reduced when adding TiO$_2$ particles to the PLA/TPS matrix, for example, T$_{max}$ decreases from 375 ^{o}C (PT 91) to 372 ^{o}C (PTT 911) and from 374 ^{o}C (PT 82) to 367 ^{o}C (PTT 821). Besides, the T$_{max}$ of the PLA/TPS/n-TiO$_2$ composites with a PLA:TPS ratio of 8:2 decreases more than that of the

composites with a PLA:TPS ratio of 9:1. This indicates a reduction in compatibility between the components in the composites. However, the T_{max} of the PLA/TPS/n-TiO$_2$ composites increases slightly with increasing n-TiO$_2$ particle content up to 2 wt.%. The results in Table 4 also show that the weight loss of the PLA/TPS/n-TiO$_2$ composites (PTT samples) at different heating temperatures is lower than that of the PLA/TPS blends (PT samples), indicating an improvement of the thermal properties of the PLA/TPS/n-TiO$_2$ composites. The remaining weight percentage of the PLA/TPS/n-TiO$_2$ composites (with a PLA:TPS ratio of 9:1) increases from 4.08 to 4.70 % when loading n-TiO$_2$ particles from 1 to 2 wt.%. This enhancement of the char formation of the PLA/TPS/n-TiO$_2$ composites is explained by the high heat resistance produced by titania itself.

The DTG curves of PLA/TPS/n-TiO$_2$ composites are presented in Figure 4. First, weight loss takes place in the temperature range from 65 to 180 ^{o}C, corresponding to the water loss from moisture. After that, there is a significant weight loss of the PLA/TPS/n-TiO$_2$ composites between 280 - 400 ^{o}C due to the decomposition of PLA.

Table 4. TG data of PLA/TPS and PLA/TPS/n-TiO$_2$ composites.

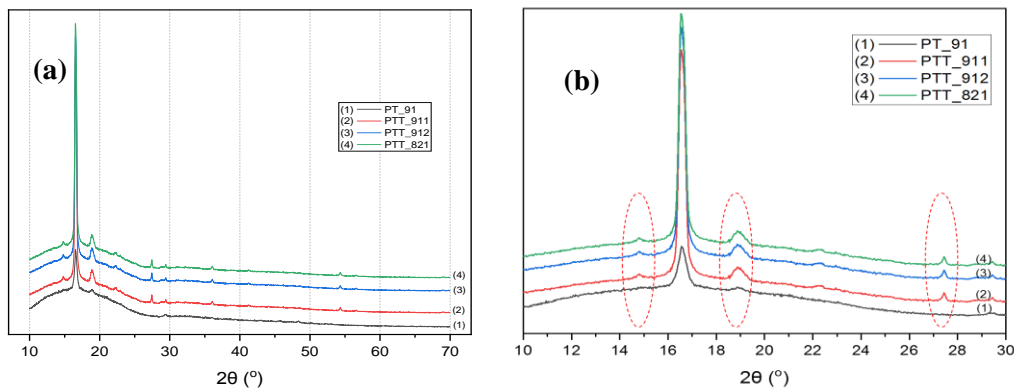| Sample	T_{on} (^{o}C)	T_{max} (^{o}C)	Remaining weight percentage (%)			
			300 ^{o}C	400 ^{o}C	500 ^{o}C	600 ^{o}C
PT 91	179	375	96.46	6.38	3.34	2.67
PT 82	177	374	93.36	9.38	3.42	2.91
PTT 911	176	372	95.53	8.62	4.88	4.08
PTT 912	178	373	95.0	7.87	5.26	4.70
PTT 821	176	367	93.59	12.21	4.86	4.32
PTT 822	176	369	93.97	12.24	5.92	5.23

3.5. XRD analysis

Figure 5. XRD curves (a) and the magnified XRD curves (b) of PLA/TPS and PLA/TPS/n-TiO$_2$ composites.

Figure 5 shows the X-ray diffraction (XRD) curves of PLA/TPS blends and PLA/TPS/n-TiO$_2$ composites loaded with n-TiO$_2$ particles with various contents. As observed in Figure 5, the peaks at approximately 16.5^o and 18.9^o have wide spreads, corresponding to the (200)/(110) and

(203) plane reflections of the orthorhombic or pseudo-orthorhombic of crystalline PLA, respectively. The XRD patterns of PLA/TPS/n-TiO$_2$ composites indicate that the crystalline structure of PLA/TPS is unchanged after combining with n-TiO$_2$ particles. In Figure 5b, comparing the XRD pattern of PLA/TPS/n-TiO$_2$ (PTT) composites with that of the PLA/TPS blends (PT 91), some new peaks at approximately 14.7^o, 22.3^o and 27.4^o in the XRD patterns of PLA/TPS/n-TiO$_2$ (PTT) composites can be observed. The appearance of these peaks may be attributed to the Ti$_2$O$_3$ phase of the titania network and the anatase or rutile phase of the crystalline structure of n-TiO$_2$ particles [23].
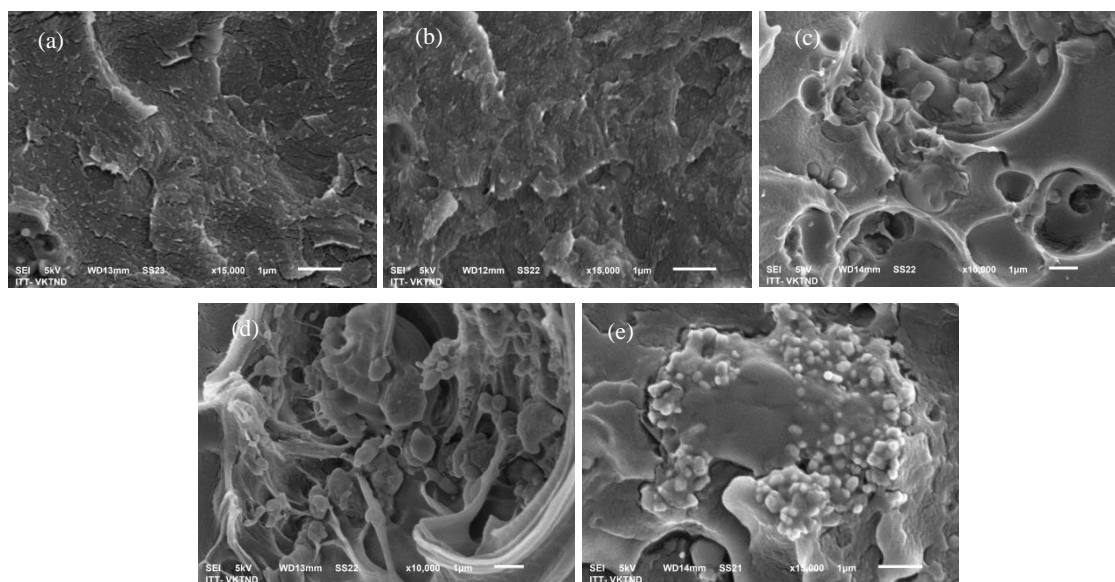
3.5. SEM images

Figure 6. SEM images of PLA-based blends with TPS and TiO$_2$: PT 91 (a), PT 82 (b), PTT 911 (c), PTT 912 (d) and PTT 821.

Figure 6 shows the SEM morphology of PLA-based blends with different contents of TPS and n-TiO$_2$ particles. From Figures 6a and 6b, it can be found that the samples have homogenous structures in a continuous phase. As seen in Figures 6c, 6d and 6e, the PLA/TPS/ n-TiO$_2$ composite structure includes two phases: matrix phase (PLA/TPS) and dispersion phase (n-TiO$_2$ particles). Most of n-TiO$_2$ particles (100 - 500 nm in size) are well dispersed in the polymer PLA/TPS matrix but with a tendency toward aggregation. The size of the agglomerates is smaller than 2 µm. The SEM image of PTT 821 indicates that n-TiO$_2$ particles are agglomerated into clusters in the PLA/TPS matrix (Figure 6e). For sample PTT 911 with a PLA:TPS ratio of 9:1, the n-TiO$_2$ particles are finely dispersed in the polymer matrix, leading to the less agglomeration of n-TiO$_2$ particles in the composites. The agglomeration of particles can be explained by the fact that the oxide particles are not surface treated.

4. CONCLUSIONS

In this work, the composites based on PLA/TPS blends and n-TiO$_2$ particles were prepared and evaluated for its characteristics. The effects of the component of the composite on the

structural, thermal behavior and tensile properties were investigated. The FTIR spectra confirmed the formation of hydrogen bond within the polymeric matrix (Ti-O-C bonds formed in the PLA/TPS matrix). The tensile properties of PLA/TPS/n-TiO$_2$ composites were strongly influenced by TPS and n-TiO$_2$ particles content. On the other hand, the results of DSC and XRD analysis showed that the simultaneous introduction of n-TiO$_2$ particles obviously increased the crystallinity of the composites (as DSC results: 40.11 % and 59.67 % corresponding to PT 91 and PTT 911, respectively). The thermal stability of PLA/TPS/n-TiO$_2$ composites was also improved due to the better dispersion and interfacial effect of n-TiO$_2$ particles with PLA/TPS matrix as shown in TGA results. The SEM images showed that n-TiO$_2$ particles were well dispersed with the matrix at a TiO$_2$ content of 1 %. However, increasing the content of TPS and n-TiO$_2$ particles leads to agglomeration, thus reducing the properties of the composite. To sum up, the properties of the PTT 911 samples are the best among all samples.

CRediT authorship contribution statement. Tran Thi Mai: Investigation, Summarization, Writing report. Nguyen Thi Thu Trang: Methodology. Nguyen Thuy Chinh: Formal analysis. Do Quang Tham: Formal analysis. Tran Huu Trung: Investigation, Methodology. Thai Hoang: Supervision.

Declaration of competing interest. The authors declare that they have no known competing financial interests or personal relationships that could have appeared to influence the work reported in this paper.

REFERENCES

1. Farah S., Anderson D. G., Langer R. - Physical and mechanical properties of PLA, and their functions in widespread applications - A comprehensive review, Adv. Drug Delivery Rev. **107** (2016) 367-392.

2. Murariu M., Dubois P. - PLA composites: From production to properties, Adv. Drug Delivery Rev. **107** (2016) 17-46.

3. Saini P., Arora M., Kumar M. N. V. R. - Poly(lactic acid) blends in biomedical applications, Adv. Drug Delivery Rev. **107** (2016) 47-59.

4. Raquez J. M., Habibi Y., Murariu M., Dubois P. – Polylactide (PLA)-based nanocomposites, Prog. Polym. Sci. **38** (2013) 1504-1542.

5. Auras R., Harte B., Selke S. - An overview of polylactides as packaging materials, Macromol. Biosci. **4** (9) (2004) 835-864.

6. Auras R. A., Lim L. T., Selke S. E., Tsuji H. - Poly(lactic acid): Synthesis, structures, properties, processing, and applications, John Wiley & Sons Inc., New York, 2011.

7. Garlotta D. - A literature review of poly(lactic acid), J.Polym. Environ. **9** (2) (2002) 63-84.

8. Jamshidian M., Tehrany E. A., Imran M., Jacquot M., Desobry S. - Poly-lactic acid: Production, applications, nanocomposites, and release studies, Compr. Rev. Food Sci. F. **9** (5) (2010) 552-571.

9. Tang X., Alavi S., Herald T. J. - Effects of plasticizers on the structure and properties of starch–clay nanocomposite films, Carbohyd. Polym. **74** (3) (2008) 552-558.

10. Teixeira E. M., Da Roz A. L., Carvalho A. J. F., Curvelo A. A. S. - The effect of glycerol/sugar/water and sugar/water mixtures on the plasticization of thermoplastic cassava starch, Carbohyd. Polym. **69** (4) (2007) 619-624.

11. Ma X. F., Yu J. G., and Wan J. J. - Urea and ethanolamine as a mixed plasticizer for thermoplastic starch, Carbohyd. Polym. **64** (2) (2006) 267-273.

12. Shi R., Zhang Z. Z., Liu Q. Y., Han Y. M., Zhang L. Q., Chen D. F., Tian W. - Characterization of citric acid/glycerol co-plasticized thermoplastic starch prepared by melt blending, Carbohyd. Polym. **69** (4) (2007) 748-755.

13. Buzarovska A., Grozdanov A. - Biodegradable poly(L-lactic acid)/TiO$_2$ nanocomposites: Thermal properties and degradation, J. Appl. Polym. Sci. **123** (4) (2012) 2187-2193.

14. Toniatton T. V., Rodrigues B. V. M., Marsi T. C. O., Ricci R., Marciano F. R., Webster T. J., Lobo A. O. - Nanostructured poly (lactic acid) electrospun fiber with high loadings of TiO$_2$ nanoparticles: Insights into bactericidal activity and cell viability, Mater. Sci. Eng. C Mater. Biol. Appl. **71** (2017) 381-385.

15. Pattamaphon C., Torpong K., Rotruedee C., Kowwit S. - Photocatalytic Oxidation of PLA/TiO2 Composite Films for Indoor Air Purification, ASC Omega **6** (16) (2021) 10629-10636.

16. Yanbing L., Yuzhen C., Gang G. - Effects of TiO$_2$ nanoparticles on the photodegradation of poly(lactic acid), J. Appl. Polym. Sci. **135** (3) (2018) 46509, doi.org/10.1002/ app.46509.

17. Pengkai W., ZhouYi X., Hanguo X., Jie C. - Synergistic effects of modified TiO$_2$/multifunctionalized graphene oxide nanosheets as functional hybrid nanofiller in enhancing the interface compatibility of PLA/starch nanocomposites, J. Appl. Polym. Sci. **137** (37) (2020) 49094-49111.

18. Gonçalves C., Pinto A., Machado A.V., Moreira J., Gonçalves I.C., Magalhães F. - Biocompatible reinforcement of poly(Lactic acid) with graphene nanoplatelets, Polym. Compos. **39** (S1) (2016) E308-E320.

19. Buasri A., Chaiyut N., Kristsanakun C., Phatkun C., Khunsri T. - Preparation and properties of nanocomposites based ond poly(lactic acid) and modified TiO$_2$, Adv. Mater. Res. **463–464** (2016) 519-522.

20. Luo Y. B., Wang X. L., Xu D. Y., Wang Y. Z. - Preparation and characterization of poly(lactic acid)-grafted TiO$_2$nanoparticles with improved dispersions, Appl. Surf. Sci. **255** (15) (2009) 6795-6801.

21. Enrica S., Antonella G., Francesca F., Vincenza A., Silvia C., Andrea L., Aurora R., Eleonora F., Carola E. C. - Biodegradable Carbon-based Ashes/Maize Starch Composite Films for Agricultural Applications, Polymers **12** (3) (2020) 524. doi.org/10.3390/ polym12030524.

22. Vitor B. C., Adriana D. C., Jose M. M., Luiz H. C. M. - Kinetics of thermal degradation applied to biocomposites with TPS, PCL and sisal fibers by non-isothermal procedures, J. Therm. Anal. Calorim. **115** (2014) 153-160.

23. Kumar P. M., Badrinarayanan S., Sastry M. - Nanocrystalline TiO$_2$ studied by optical, FTIR and X-ray photoelectron spectroscopy: correlation to presence of surface states, Thin Solid Films **358** (1-2) (2000) 122-130.